Understanding the fundamental principles of metal oxide based gas sensors; the example of CO sensing with SnO_2 sensors in the presence of humidity

2003 J. Phys.: Condens. Matter 15 R813

(http://iopscience.iop.org/0953-8984/15/20/201)

INSTITUTE OF PHYSICS PUBLISHING JOURNAL OF PHYSICS: CONDENSED MATTER

J. Phys.: Condens. Matter **15** (2003) R813–R839 PII: S0953-8984(03)33587-8

TOPICAL REVIEW

Understanding the fundamental principles of metal oxide based gas sensors; the example of CO sensing with SnO_2 sensors in the presence of humidity

N Bârsan and U Weimar

Institute of Physical and Theoretical Chemistry, University of Tübingen, Auf der Morgenstelle 8, D-72076 Tübingen, Germany

Received 8 February 2003
Published 12 May 2003
Online at stacks.iop.org/JPhysCM/15/R813

Abstract

This paper investigates the effect of water vapour in CO sensing by using Pd doped SnO_2 sensors realized in thick film technology as an example of the basic understanding of sensing mechanisms applied to sensors. The results of phenomenological and spectroscopic measurement techniques, all of them obtained under working conditions for sensors, were combined with modelling in order to derive conclusions able to be generalized to the field of metal oxide based gas sensors. The techniques employed were: dc conductance, ac impedance spectroscopy, work function (by using the Kelvin probe method), catalytic conversion and diffuse reflectance infrared Fourier transform measurements. The most important conclusion is that the different parts of the sensor (sensing layer, electrodes, substrate) are all influencing the gas detection and their role has to be taken into consideration when one attempts to understand how a sensor works.

(Some figures in this article are in colour only in the electronic version)

Contents

1. Introduction

This contribution uses mainly results obtained in the last few years by the Gas Sensor Group at the University of Tübingen in an attempt to understand metal oxide based gas sensors. The reason for starting this work was the finding that a fractal knowledge is the result of research and development in this field. Accordingly, the aim was to put together a research approach that results in a coherent picture integrating both a basic understanding and sensor application aspects. The approach/research program was first outlined in [1]. Its rationale is presented in the following:

- Assessment of the state of the art by a literature survey and selection of an appropriate metal oxide system. The candidate used for this is SnO_2.
  SnO_2 is a wide bandgap n-type semiconductor, its conduction type being related to the intrinsic oxygen vacancies. Gas sensors based on this material are extensively used in the detection of toxic gases. Their advantages, such as low cost and high sensitivity, make them very attractive, whereas their disadvantages, such as lack of selectivity and the strong interfering effect of water vapour, still hinder their use as measuring devices.
- Definition of objectives for the next steps:
  - ∗ What are the relevant parameters to be focused on?
    - + Identification of relevant problems, e.g. CO in the presence of humidity.
    - + Typical 3S parameters (stability, sensitivity, selectivity) as a basis for benchmarking.
  - ∗ What are the experimental and boundary conditions?
    - + Measure as much as possible in real world conditions and on real world samples. This will lead to measurements performed under gas atmospheres provided by gas mixing stations. Most of the measurements are electrical measurements and optical spectroscopy. For material characterization tasks UHV techniques were also used.
- Preparation of appropriate samples according to the following criteria:
  - ∗ 'Simple' preparation of sensitive material, which avoids additives (where the additive role is not quite understood).
  - ∗ Very sensitive samples to get sufficient 'effect' (good signal to noise ratio).
  - ∗ Optimized substrate (materials).
  - ∗ Solid experimental basis: high throughput reproducible preparation method, which ensures a high sample to sample reproducibility and consequently allows for testing of devices in totally different experimental rigs in different laboratories over a long period.

- Extensive testing for selection of appropriate combinations of samples and relevant parameters. Anticipating a little bit, the main conclusions were:
  - The home-made SnO_2-based sensors live up to the standards of commercial SnO_2-based sensors. In particular, the ones doped with 0.2 wt% Pd showed excellent sensitivity for CO detection and remarkable long-term stability and have been chosen for the following basic studies.
  - CO detection is especially influenced by the presence of humidity. Consequently, the water–CO combination was used as a model system.
- Selection of complementary experimental techniques appropriate to the above mentioned research approach.
  - DC resistance measurements are the 'normal' way for sensor measurements and allow for the screening of a large number of sensors.
  - AC impedance spectroscopy as a technique which is applied in normal operation conditions. AC impedance spectroscopy provides knowledge on the different contributions (surface, bulk, contact) to gas sensing.
  - Work function change measurements by the Kelvin method are also performed in normal operation conditions. They additionally provide insight about surface reactions where free charge carriers are not involved.
  - Catalytic conversion measurements in normal operation conditions give additional information about the gas sensing reaction paths.
  - Infrared spectroscopy, and especially DRIFT measurements, are allowing (in principle) the identification of the surface species involved in the sensing process in normal operation conditions. It is one of the few spectroscopic techniques which can be applied in normal operation conditions.
- Development of the necessary tools for the interpretation of the experimental findings; the modelling should start from elementary steps governing those surface–molecule interactions which lead to charge transfer (adsorption, reaction, desorption, etc) and then show how these steps are linked with the macroscopic parameters describing the sensor response.
- Application of the interpretation tools to precisely planned experimental model systems.

Most of the experimental techniques were used in the past for studying gas sensors [2–13]. However, they were never combined and applied to the same samples/sensors and their results never integrated into a complete modelling of gas sensing.

Partly, the experimental results and the modelling tools are already published [14–18] or submitted for publication [19, 20]. Nevertheless, the general picture became clearer just recently and it was not reported up to now. In the following, the approach is demonstrated in a step by step manner.

2. Experimental details

2.1. Sample preparation

The sensing material is based on a nanocrystalline tin oxide powder. As a starting point, $Sn(OH)_4$ is precipitated by adding ammonia to an aqueous solution of tin chloride. After a washing step, the precipitate is calcined at 450 °C for 8 h. The surface doping (0.2 wt% Pd) of the final sensing material is realized by powder impregnation using the corresponding metal chloride. An additional heat treatment (450 °C for 1 h) reduces the metal chloride to metallic Pd and removes the chlorine. Afterwards, the powder is mixed with an appropriate

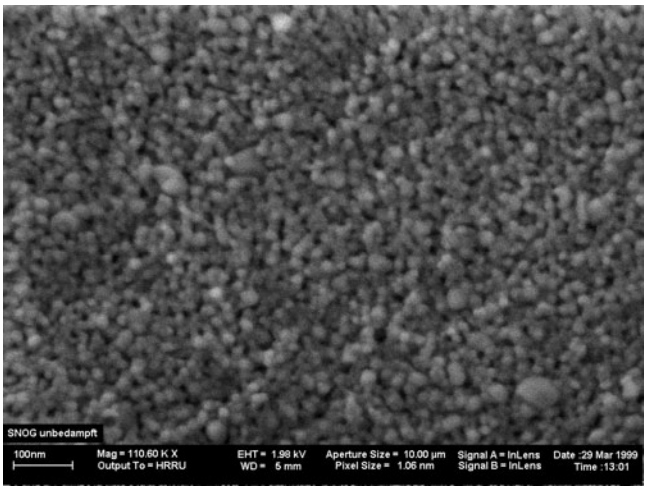

Figure 1. SEM pictures of the SnO_2 sensing layer.

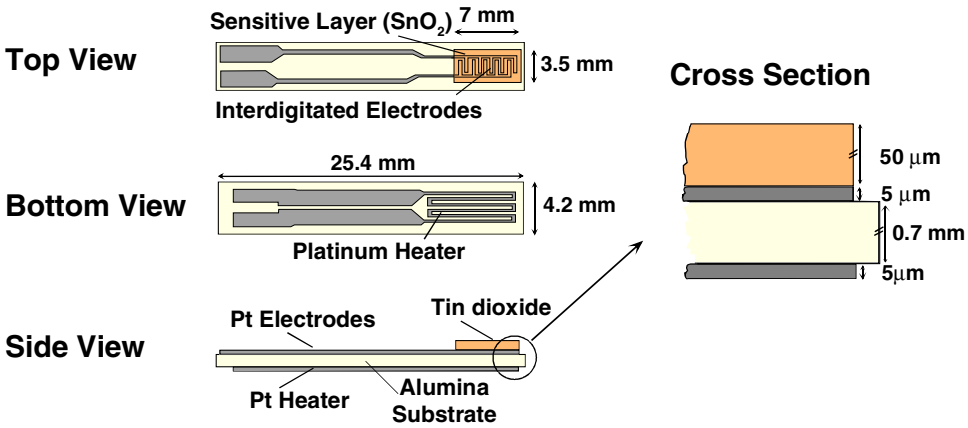

Figure 2. Layout of the planar alumina substrate with Pt electrodes and Pt heater. The SnO_2 layer is printed on top of the interdigitated electrodes. The heater on the back keeps the sensor at the operational temperature.

mixture of solvents (mainly propandiol) until a homogeneous, printable paste is obtained. The paste is afterwards transferred onto an planar alumina substrate by an automatic screen printer (EKRA Microtronic II). The front side of the alumina substrate is provided with interdigitated electrodes onto which the paste is deposited. The Pt heater on the backside of the substrate enables the operation of the sensor at a well-controlled temperature. The final annealing (700 °C for 10 min) removes the solvent and binds the sensing layer to the substrate. Figure 1 shows a SEM picture of the resulting sensing layer. Figure 2 shows a schematic of the sensors used in this work. A complete microstructural characterization of the sensing material is given in [21]. A presentation of the gas sensing performance and the long-term behaviour of the sensors is given, for example, in [22].

2.2. DC measurements

The typical measurement technique for metal oxide sensors is the measurement of conductance or resistance. In this work dc measurements were performed by using electronic circuitry which ensures a constant voltage drop over the sensing layer. With such a technique, a defined polarization and a known and constant measurement potential, were ensured. In this way, effects of the possible influence of the measuring potential, like the ones already reported for very similar samples, were avoided [23]. The measuring potential was adjusted in a range in which its influence on the measurement is minimal.

2.3. Catalytic conversion measurements

The catalytic conversion of CO to CO_2 during the gas sensing with SnO_2-based sensors was monitored by using a combination of liquid amperometric CO sensors (EC) and IR CO_2 sensors (for details, see [17]). The gas mixtures produced by a gas flow system were successively delivered to: first to the EC and then to the sensors and, afterwards, first to the sensors and then to the EC. The differences in the signal of the EC were used to calculate the amount of CO catalytically converted to CO_2 and the IR CO_2 sensor was used as an additional checking method. The absence of any other reaction products was previously checked by a FTIR spectrometer.

2.4. Work function change measurements

The technique used here for measuring differences in work functions is the well established Kelvin oscillator method [24, 25]. In our case, the Kelvin oscillator consists of a metallic grid in electrical contact with the sample, which oscillates at a mean distance d over the sample. Due to the electrical contact, a contact potential V_C, which is equal to the difference in work function of the two materials $\Delta\Phi$, occurs. This results in an electrical field between the two plates of the capacitor, the sample and the grid. Changes in distance due to the oscillation result in changes of the capacity C and therefore in a current $i(t)$ according to

$$C(t) = \varepsilon\varepsilon_0 A/(d_0 + \delta \sin \omega t) = Q(t)/V_C \tag{1}$$

$$i(t) = \dot{Q} = -V_C \varepsilon\varepsilon_0 A\delta\omega \cos \omega t/(d_0^2(1 + \delta/d_0) \sin \omega t)^2. \tag{2}$$

Experimentally, a counter-voltage V_G is adjusted until $i(t)$ disappears and the contact potential $V_C = -V_G = \Delta\Phi$ is measured (for details see figure 3). Consequently, if the work function of the metallic grid is unaffected by changes in the ambient atmosphere it is possible to determine the work function changes of the sample dependent on gas adsorption.

2.5. Impedance spectroscopy measurements

For the measurements a Hewlett-Packard impedance analyser (HP 4194A) was used in combination with a self-made test fixture designed for the auto-balancing bridge method. The analyser allows us to measure in the frequency range between 100 Hz and 40 MHz and to perform open/short compensation for the whole frequency range in one run. The home-made test fixture, in fact a gas-tight test chamber provided with gas inlet and outlet, allowed the plugging in of the sensor by using a standard connector. Comparison of the results obtained by measuring standard resistances and capacitances with the test fixture provided by Hewlett-Packard and with the home-made test fixture did not show significant differences. For details see also [20].

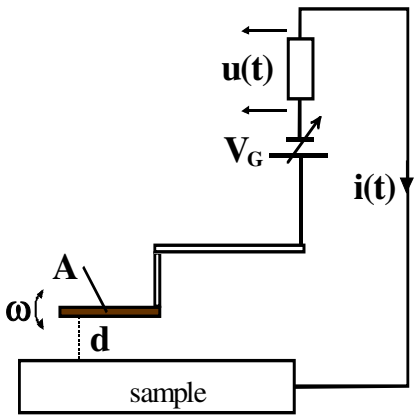

Figure 3. Principal set-up of a Kelvin probe. A metallic grid oscillates over a sample. The counter-voltage V_G is adjusted in such a way that the current i vanishes.

2.6. DRIFT measurements

Among the spectroscopic techniques, needed to be applied in order to validate the phenomenological results, infrared spectroscopy seems to be the most suitable for experiments performed under realistic operation conditions. Due to its nature, as most of the signal comes from indirect reflections and its good sensitivity in the spectral range where interesting surface species are found, DRIFT is particularly suitable for application to studies of surface phenomena and large specific surface materials such as the sensing layers we are interested in. In our experiments, the sensors were placed in a special home-made sensor chamber, which allows for:

- a maximum of diffuse reflectance from the sensor surface due to the presence of windows through which the IR incident beam could enter and the diffuse reflected beam could reach the DRIFT optical system.
- the exposure of the sensor to different gas mixtures due to the possibility of connecting the tight sensor chamber to a gas flow system and purging it with the desired gas mixtures.
- the sensor chamber being placed in the DRIFT unit of an evacuable Bruker IFS 66v FTIR spectrometer, which allowed for recording spectra at a spectral resolution of 2 cm^{-1} and 1024 scans. For more details on the experimental procedure see [19].

2.7. Gas tests

The adjustment of the desired gas mixtures was performed by means of a gas flow system with computer-driven mass flow controllers. The humidity was adjusted by bubbling synthetic air through a column of water and subsequently mixing it with dry air in a gas blender. Between two successive exposures to test gases the sensors were purged for 1 h with background gas (dry or humidified synthetic air) to allow the sensors to recover.

3. Results and discussion

3.1. CO sensing and transduction—state of the art

Tin oxide sensors are generally operated in air in the temperature range between 200 and 400 °C. At these temperatures it is generally accepted that the conduction is electronic; it is also accepted

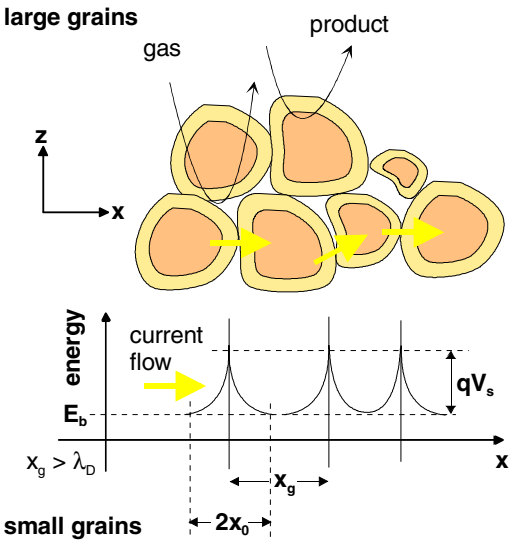

Figure 4. Schematic representation of a porous sensing layer with geometry and energy band. λ_D is the Debye length, x_g is the grain size and x_0 is the depth of the depletion layer.

that chemisorption of atmospheric gases takes place at the surface of the tin oxide. The overall conduction in a sensor element, which will determine the sensor resistance, is determined by the surface reactions, the resulting charge transfer processes with the underlying semiconducting material and the transport mechanism from one electrode to the other through the sensing layer (the latter can even be influenced by the electrical and chemical electrode effects). For example, it is well known and generally accepted that the effect of oxygen ionosorption as O_2^- or O^- will be the building of a negative charge at the surface and the increase of the surface resistance [1, 26–28]. It is also considered that reducing gases like CO react with the surface oxygen ions, freeing electrons—the sensing step—that can return to the conduction band. The transduction step, i.e. the actual translation of this charge transfer into a decrease of the sensor resistance, depends (as shown in [14]) on the morphology of the sensing layer. The result is that, even for exactly the same surface chemistry, the dependence of the sensor resistance on the concentration of CO can be very different for compact and porous sensing layers (as defined in [14]).

In our case, the sensing layer consists of single crystalline grains with a narrow size distribution (see figure 1 and [21]). Due to the fact that the final thermal treatment is performed at 700 °C, the grains are just loosely connected. Accordingly, the best way to describe the conduction process is to consider that the free charge carriers (electrons for SnO_2) have to overcome the surface barriers appearing at the surface of the grains (see figure 4 and [14]). Due to the narrow size distribution it is also quite probable that a mean-field treatment suffices and there is no need for Monte Carlo simulations or percolation theory. One can easily model the dependence of the resistance on the CO concentration by making the following assumptions, supported by the already established knowledge in the field:

- The reaction of CO takes place just with the previously adsorbed oxygen ions (well documented for the temperature and pressure range in which the gas sensors operate).
- The adsorption of CO is proportional to the CO concentration in the gas phase (quite reasonable but never really experimentally proved).

On the basis of the a.m. assumptions one can combine quasi-chemical reaction formalism with semiconductor physics calculations and one obtains power-law dependences of the form

$$R \sim p_{\mathrm{CO}}^{n} \tag{3}$$

where the value of n depends on the morphology of the sensing layer and on the actual bulk properties of the sensing materials (see a complete analysis in [14]). The relationship described by equation (3) is well supported by experiments.

In order to verify the validity of the modelling, it is very important to check whether the assumption of the proportionality between the adsorbed and gaseous CO is valid; this is one of the objectives of our experimental studies.

For the effect of water vapour on the resistance of tin oxide based gas sensors there are a couple of ideas, briefly presented below (for details see [14]). There are three types of mechanisms to explain the experimentally proven increase of surface conductivity in the presence of water vapour. Two, direct mechanisms, are proposed by Heiland and Kohl [29] and the third, indirect, is suggested by Morrison and by Henrich and Cox [30, 31].

The *first mechanism* of Heiland and Kohl attributes the role of the electron donor to the 'rooted' OH group, the one including lattice oxygen. The equation proposed is

$$\mathrm{H_2O}^{gas} + \mathrm{Sn_{Sn}} + \mathrm{O_O} \rightleftharpoons (\mathrm{Sn}_{\mathrm{Sn}}^{\delta+} - \mathrm{OH}^{\delta-}) + (\mathrm{OH})_{\mathrm{O}}^{+} + \mathrm{e}^{-} \tag{4}$$

where $(\mathrm{Sn}_{\mathrm{Sn}}^{\delta+} - \mathrm{OH}^{\delta-})$ is referred to as an isolated hydroxyl or OH group (dipole) and $(\mathrm{OH})_{\mathrm{O}}^{+}$ is the rooted one. In the first equation, the donor is already ionized.

The reaction implies the homolytic dissociation of water and the reaction of the neutral H atom with the lattice oxygen. The latter is normally fixing two electrons and then consequently being in the $(2-)$ state. The built-up rooted OH group, having a lower electron affinity, can become ionized and become a donor (with the injection of an electron into the conduction band).

The *second mechanism* takes into account the possibility of the reaction between the hydrogen atom and the lattice oxygen and the binding of the resulting hydroxyl group to the Sn atom. The resulting oxygen vacancy will produce, by ionization, the additional electrons. The equation proposed by Heiland and Kohl [29] is

$$\mathrm{H_2O}^{gas} + 2\mathrm{Sn_{Sn}} + \mathrm{O_O} \rightleftharpoons 2(\mathrm{Sn}_{\mathrm{Sn}}^{\delta+} - \mathrm{OH}^{\delta-}) + \mathrm{V}_{\mathrm{O}}^{2+} + 2\mathrm{e}^{-}. \tag{5}$$

Morrison, as well as Henrich and Cox [30, 31], consider an indirect effect more probable. This effect could be the interaction between either the hydroxyl group or the hydrogen atom originating from the water molecule with an acid or basic group, which are also acceptor surface states. Their electronic affinity could change after the interaction. It could also be the influence of the co-adsorption of water on the adsorption of another adsorbate, which could be an electron acceptor. Henrich and Cox suggested that the pre-adsorbed oxygen could be displaced by water adsorption. In any of these mechanisms, the particular state of the surface plays a major role, due to the fact that it is considered that steps and surface defects will increase the dissociative adsorption. The surface dopants could also influence these phenomena; Egashira *et al* [32] showed by TPD and isotopic tracer studies combined with TPD that the oxygen adsorbates are rearranged in the presence of adsorbed water. The rearrangement was different in the case of Ag and Pd surface doping.

In choosing between one of the proposed mechanisms, one has to keep in mind that:

- in all reported experiments, the effect of water vapour was the increase of surface conductance,
- the effect is reversible, generally with a time constant of the order of around 1 h.

It is not easy to quantify the effect of water adsorption on the charge carrier concentration, n_S (which is normally proportional to the measured conductance). For the first mechanism of water interaction proposed by Heiland and Kohl ('rooted', equation (4)), one could include the effect of water by considering the effect of an increased background of free charge carriers on the adsorption of oxygen.

For the second mechanism proposed by Heiland and Kohl ('isolated', equation (5)) one can examine the influence of water adsorption (see [33]) as an electron injection combined with the appearance of new sites for oxygen chemisorption; this is valid if one considers oxygen vacancies as good candidates for oxygen adsorption. In this case one has to introduce the change in the total concentration of adsorption sites $[S_t]$:

$$[S_t] = [S_{t0}] + k_0 p_{H_2O} \tag{6}$$

obtained by applying the mass action law to equation (5). $[S_{t0}]$ is the intrinsic concentration of adsorption sites and k_0 is the adsorption constant for water vapour.

In the case of the interaction with surface acceptor states, not related to oxygen adsorption, one can proceed as in the case of the first mechanism proposed by Kohl. In the case of an interaction with oxygen adsorbates, one can consider that the dissociation of oxygen ions is increased and examine the implications.

Due to the large effort implied by the modelling, it is important to find out which of the proposed mechanisms is the important one. This is also an objective of the experiments to be presented in what follows.

The influence of water vapour on CO detection is well documented (see, for example, [16, 33–39]). Generally the papers are just describing the effects without going too far into the modelling/explanation of the effects. When they provide models, they are not based on the combination of spectroscopic and phenomenological measurement techniques applied in realistic sensor operation conditions, as presented here. The explanations span between considering OH groups as weak acceptors, competing with oxygen for the same adsorption sites and more easily accessible to the reaction with CO [28] to a complete decoupling between the CO and water surface reactions [35, 38]. Anyhow, the active surface species related to water vapour are considered to be the hydroxyl groups.

3.2. DC measurements

The results obtained by dc characterization of Pd doped sensors can be summarized as follows. With increasing humidity:

- the resistance in air decreases,
- the resistance in the presence of CO decreases,
- the sensor signal to CO increases,
- the calibration curves and the corresponding sensor signals can be approximated by power laws.

These facts are not surprising and are very similar to the ones generally reported. Interesting findings are shown in figures 5 and 6; figure 5 shows two types of normalized sensor signal dependences on CO concentration (in the range 50–500 ppm) for 0 and 50% relative humidity. The sensor resistance is either related to the sensor resistance in the absence of CO (S1) or to the sensor resistance in the presence of a fixed CO concentration (S2).

The difference in the dependence on humidity is quite striking. The sensor signals S1 for 0 and 50% relative humidity differ strongly, whereas the sensor signals S2 overlap completely in the presence of CO. When the normalization procedure S2 is applied to the resistance data

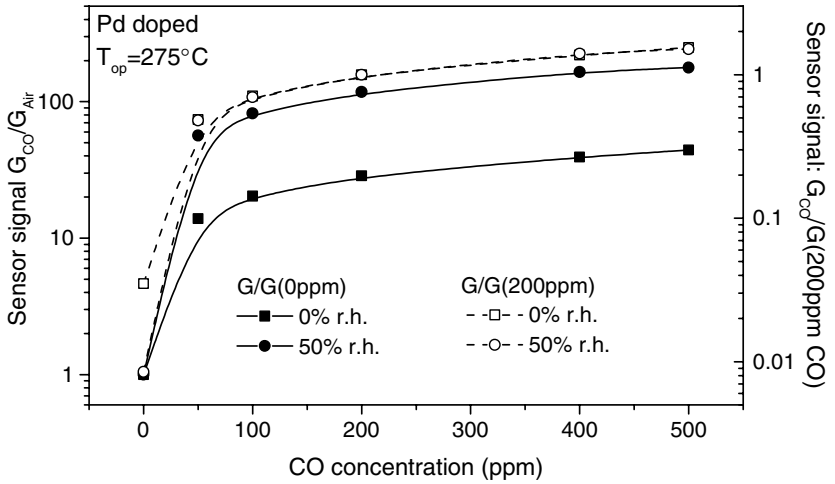

Figure 5. Sensor signal dependence on CO concentration of Pd doped sensors in dry air (□ and ■) and at 50% relative humidity (○ and ●). The two normalization procedures are performed with respect to the resistance in the absence of CO (full curves) and in the presence of 200 ppm CO (broken curves).

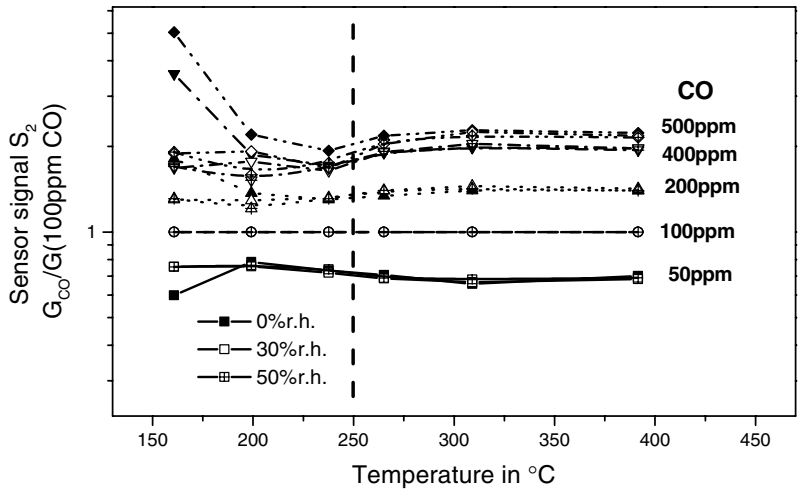

Figure 6. Normalized sensor signal S_2 ($G_{CO}/G(100\ \text{ppm CO})$) as a function of operational temperature. The Pd doped sensors have been characterized for operational temperatures between 150 and 400 °C, the ambient humidity was varied between 0 and 50% relative humidity, the CO concentration was between 50 and 500 ppm. Above 250 °C, S_2 is independent of the ambient humidity and hardly dependent on the operational temperature.

obtained at the various operational temperatures (250–400 °C) it does not only work for each single temperature, but also all resulting sensor curves overlap. This is illustrated in figure 6. The normalization S2 completely eliminates the influence of water for CO concentrations in the range 50–500 ppm and temperatures between 250 and 400°C. These findings suggest that CO reacts at the surface of the Pd doped sensors with water-related species and, as is generally accepted, with oxygen ions; it seems that the reaction with the water-related species is limited to concentrations below 50 ppm CO and that, in terms of the influence on conductance, its effect appears as a constant multiplicative term at concentrations above 50 ppm CO.

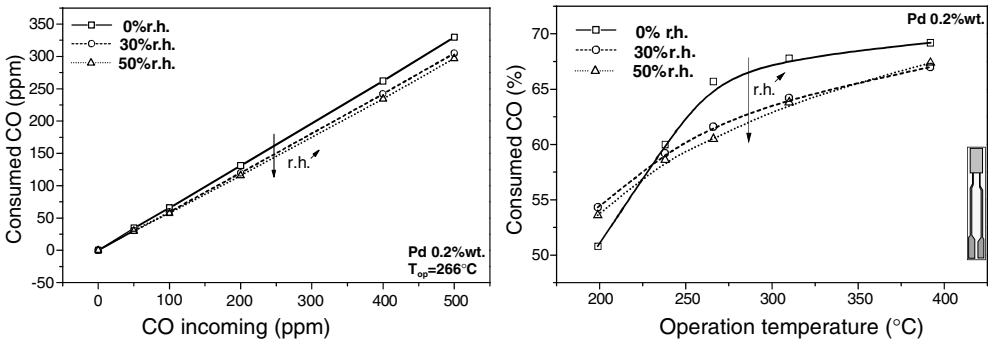

Figure 7. CO consumption by Pd doped sensors. Left: dependence of CO consumption on the ambient humidity for $T_{op} = 270\,^{\circ}\mathrm{C}$. The CO consumption of the sensors is linear and decreases with increasing humidity. Right: summary of CO consumption dependence on the operational temperature and ambient humidity. CO consumption increases with the operational temperature and decreasing humidity.

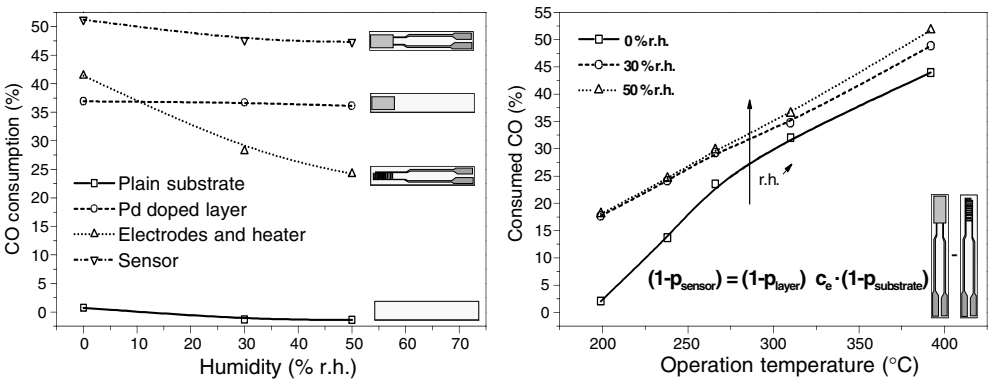

Figure 8. CO consumption related to the individual sensor parts of Pd doped thick film sensors. Left: CO consumption related to the bare alumina substrates, alumina substrates with Pt electrodes and heater, alumina substrates with sensitive layer on top, and consumption of sensors. Right: consumption related to the sensitive layer as calculated from the consumption data for sensors and the consumption data for substrates provided with electrodes and heater.

The results also support the idea that in this temperature range CO interacts with only one type of ionosorbed oxygen species, probably O^-; otherwise reactions with different ionosorbed species would determine different relationships between sensor resistance and CO concentration [14], i.e. different slopes for sensors and no overlapping curves as shown in figure 6.

3.3. Catalytic conversion measurements

The main results obtained by studying the catalytic conversion of CO to CO_2 during sensing are presented in figures 7 and 8 (a detailed presentation can be found in [17]). One can observe that the CO consumption is a linear phenomenon, which increases when the temperature is increased and the humidity is decreased (see figure 7). The linearity of the consumption relation suggests that the assumption of a linear relationship between gaseous and adsorbed CO is correct and, as a consequence, the non-linearity of the dependence of the resistance/conductance is indeed

determined by the transduction. The increase of the catalytic conversion by the increase of the operational temperature is not surprising. What is really surprising, at least at a first glance, is the decrease of consumption due to the increase of humidity. One would expect that, due to the fact that the increase in humidity determines an increase of the sensor signal and that an increased sensor signal means more sensing reactions, the associated CO consumption should also increase. This fact signals that a sensor, being a complex device, means there are additional phenomena that result in CO consumption without an electrical/sensor signal counterpart. To clarify that aspect, the catalytic conversion associated with the different sensor parts was investigated (figure 8, left). One can see that the bare alumina substrates show—within the precision of the measurement—no CO consumption. Substrates provided with electrodes and a heater show a significant consumption, which strongly decreases with humidity. Alumina substrates with a sensitive layer on top also show strong consumption but no measurable dependence on humidity, although we expected an increase in consumption with increasing ambient humidity. Finally, the consumption of sensors is remarkably large and decreases with increasing humidity. These findings suggest that the humidity influence is not related to the sensing material alone but to a combination of the substrate and the electrode-sensing material. One could assume that the consumption of the sensors is an independent overlapping of the consumption of the sensitive layer and the substrate provided with electrodes and heater. However, any attempts to apply such a reasoning for calculation of the CO consumption of the sensors as a sum of the consumption associated with its constituents failed. As a consequence, one can conclude that the consumption of the sensor is not just the sum of the independent contributions of the sensitive layer and the substrate. The substrate and the sensitive layer interact in some way. If one calculates the contribution to the CO consumption that is due to the sensing layer–electrode combination one finds that it is increases with increasing humidity, which is in line with the humidity influence on the sensor signal (figure 8, right).

3.4. Work function change measurements

By performing simultaneous conductance/resistance and work function measurements one can get information about the changes in surface concentration species that are not carrying a net charge, such as dipoles. This is of special interest when one studies the effect of water vapour because their surface interaction can lead to such species (see equation (4)). This happens because work functions Φ of semiconductors contain three contributions: the energy difference between the Fermi level and conduction band in the bulk $(E_C - E_F)_b$, band bending qV_S and electron affinity χ (equation (8) and figure 9). All three contributions may, in principle, change upon gas exposure:

$$\Phi = (E_C - E_F)_b + qV_S + \chi. \tag{7}$$

The corresponding conductance G may formally be described by equation (8) (see, for example, [14]); here we assume that the work function changes measured by the Kelvin probe at the outer layers are identical with the electrostatic potential changes involving the inner grains. The latter control the conduction changes upon gas exposure; one also assumes a narrow size distribution of the electrically active grains in the sensing layer and hence homogeneous electrical properties, percolation paths of the conductivity independent of the work function changes, and constant mobility of the charge carriers in the nanoparticles:

$$G = G_0 \exp\left\{\frac{(E_F - E_C)_b - qV_S}{kT}\right\} = G_0 \exp\left\{\frac{\chi - \Phi}{kT}\right\}. \tag{8}$$

It is worth mentioning that changes in the electron affinity χ influence the work function Φ but not the electrical conductance G.

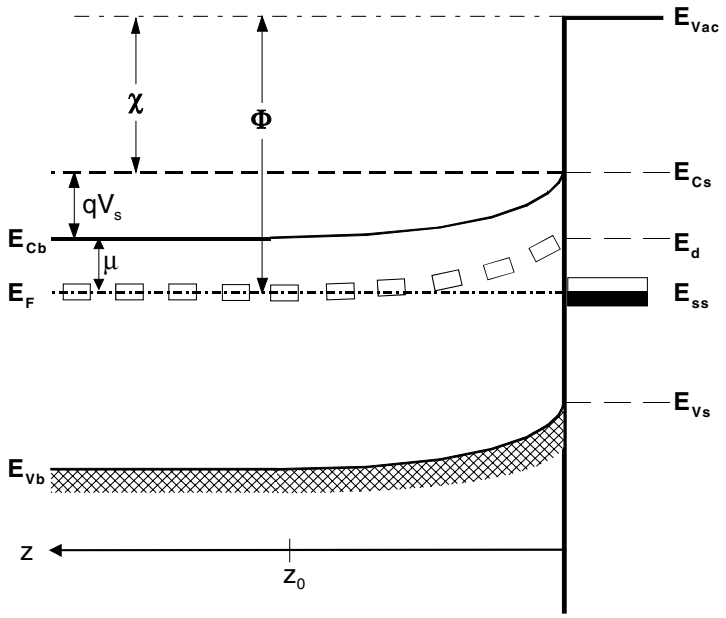

Figure 9. Band bending after chemisorption of charged species (e.g. ionosorption of oxygen on E_{SS} levels). Φ denotes the work function, χ is the electron affinity and μ is the electrochemical potential.

By combining equations (7) and (8), it gives that

$$kT \ln G/G_0 = \chi - \Phi. \tag{9}$$

If the sensors are exposed to two different gas atmospheres (initial gas atmosphere I and final gas atmosphere F) and the related resistances (R_I, R_F) and work functions (Φ_I, Φ_F) are monitored, the different contributions to the work function change, $\Delta\Phi$, can be determined according to

$$\Phi_{I,F} = -kT \ln(G_{I,F}/G_0) + \chi_{I,F}. \tag{10}$$

Hence

$$\Delta\Phi = \Phi_F - \Phi_I = kT \ln(G_I/G_F) + \chi_F - \chi_I = kT \ln(R_F/R_I) + \Delta\chi \tag{11}$$

where Φ_I, R_I and χ_I are the work function, the resistance and the electron affinity in the initial gas atmosphere, respectively, and Φ_F, R_F and χ_F are the corresponding values in the final gas atmosphere. In all our experiments $\Delta\Phi$ and the electrical resistance were measured and, by using equation (12), $\Delta\chi$ was calculated.

In order to characterize the influence of water only, the sensors (operated at 270 °C) were exposed to an atmosphere with different concentrations of water vapour. The results are presented in figure 10. An increase in humidity results in a decreased resistance and an increased electron affinity χ. Affinity changes may formally be attributed to changes in the coverage and/or absolute value of dipoles oriented perpendicular to the surface [40]. The observed increase in electron affinity and the decrease in resistance (band bending) with increasing humidity can be explained by an increased coverage of surface hydroxyl groups as suggested by the mechanisms proposed by Heiland and Kohl ([29] and equations (4) and (5)) and the appearance of donors. It is still not possible to decide between the two models because

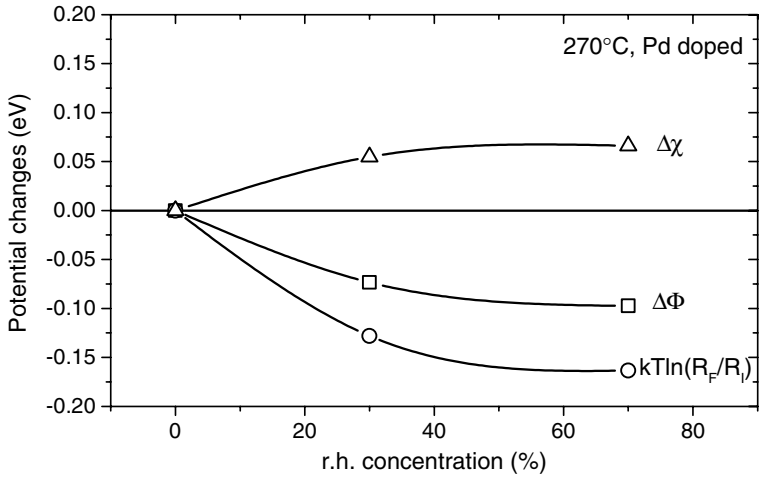

Figure 10. Typical potential changes of Pd doped sensors upon water vapour exposure determined here at 270 °C. For the definition of the three contributions, see the text.

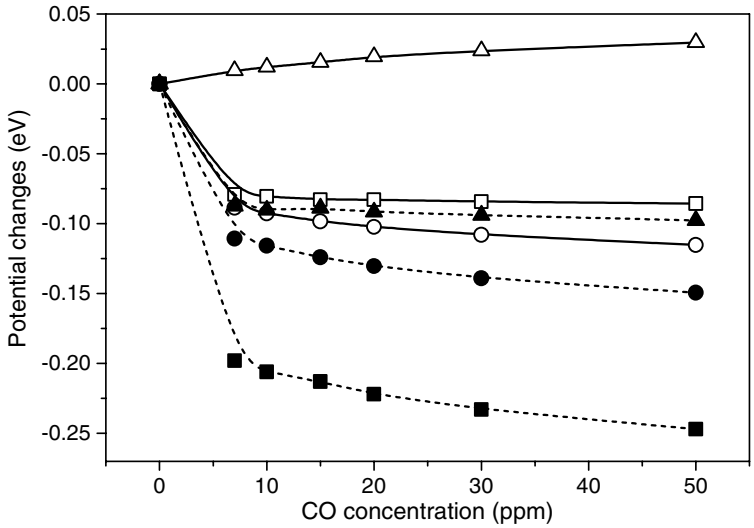

Figure 11. Typical potential changes upon CO exposure determined at 270 °C using Pd doped sensors (a) in dry air (□ indicates $\Delta\Phi$, ○ indicates $kT\ln(R_F/R_I)$, △ indicates $\Delta\chi$) and (b) at 50% relative humidity (■ indicates $\Delta\Phi$, ● indicates $kT\ln(R_F/R_I)$, ▲ indicates $\Delta\chi$).

one cannot differentiate, with phenomenological techniques, between the different ways in which the donors are produced; one can just record the effects, namely the decrease of the resistance.

To further investigate the CO–water interaction, simultaneous work function and resistance measurements have been performed in a background of both humidified and dry synthetic air. Figure 11 shows typical results of the influence of water during CO exposure. For zero humidity the electron affinity χ did not change (within the precision of the measurement). In the presence of water the electron affinity changes dramatically upon exposure to CO even at very low concentrations and remains almost constant for higher CO concentrations. The decrease

of the electronic affinity can be attributed to a decrease of the concentration of isolated surface hydroxyl groups associated to a reaction with CO. It was proposed in [15] that, following a reaction of CO with the oxygen of the isolated hydroxyl group, the freed H atom could build up a donor in a similar way as the one in which donors were built by hydrogen atoms resulting from the dissociation of the water molecule. In the case of the first mechanism (equation (4)) this decrease in electron affinity may be explained by the decrease of the concentration of surface dipoles, attributed to $(Sn^{+}_{Sn} - OH^{-})$, and the observed resistance decrease by the generation of additional 'rooted' OH groups:

$$CO^{gas} + (Sn^{+}_{Sn} - OH^{-}) + O_O \rightarrow {CO_2}^{gas} + Sn_{Sn} + (OH)^{+}_{O} + e^{-} \quad (12)$$

whereas in the case of the second mechanism (equation (5)), one would have to assume that

$$CO^{gas} + (Sn^{+}_{Sn} - OH^{-}) + O_O \rightarrow {CO_2}^{gas} + (Sn^{+}_{Sn} - OH^{-}) + V^{2+}_{O} + 2e^{-}. \quad (13)$$

For the second case, the electron affinity would not change, which contradicts the experimental observations. This strongly suggests that the mechanism of water adsorption is the one described by equation (4). The reaction of equation (12) occurs in addition to the reaction of CO with ionosorbed oxygen. The proposed mechanism explains the sensitization effect of water on CO detection by the fact that an increased humidity results in an increased concentration of surface dipoles and thus in an increased number of reaction partners (hydroxyl groups) and an increased efficiency in the CO reaction.

The impact of the CO–water reaction seems to decrease strongly with increasing CO concentration; above 10 ppm CO, there are only small changes in the electron affinity. The same behaviour is also observed at higher temperatures up to 400 °C but, due to the thermal decomposition of OH groups, the corresponding absolute changes in $\Delta\chi$, as well as the sensitivity to CO, decrease. It looks like the difference in CO sensitivity for this type of sensor, doped with Pd, when the temperature or the dopant concentration changes, is mainly related to the changes in the interaction with water vapour. The results of work function change measurements provide a more solid basis for the findings of dc measurements alone.

For a confirmation of the results one can evaluate the change in surface dipole coverage ($\Delta\theta$); this can be determined by means of the following equation (see [40]):

$$\Delta\chi = \frac{q}{\varepsilon_S \varepsilon_0} \Delta\theta N^{ad}_{(S)max} \bar{\mu}^{ad}. \quad (14)$$

With the assumptions that $N^{ad}_{(s)max} \approx 10^{19}$ m^{-2} (surface density of tin atoms), $\bar{\mu}^{ad} \approx 1.66$ D $= 1.66 \times 3.3 \times 10^{-30}$ C m [5] and $\varepsilon_S = \varepsilon_{SnO_2}/(2)^{0.5} = 8.5$, the changes in dipole coverage are in the range of fractions of a monolayer (ML). Bearing in mind that, for hydroxyl groups, TDS coverage experiments indicate a surface coverage of about 15% of a ML [41], the results seem quite reasonable.

3.5. Impedance spectroscopy measurements

Impedance spectroscopy is an useful tool for the identification of different elements of a complex device, such as a thick film gas sensor. In figure 12 the different elements possible to be present in our gas sensors are shown together with their ac equivalent circuits and their dependence on the main parameters that might be influenced by the different ambient atmospheric conditions (V_S and ε: for details see [20]). As has been discussed before, the sensitive layer of the sensors consists of interconnected tin dioxide grains. In the presence of oxygen the surface layer of every grain becomes depleted of charge carriers and, in the case of $\lambda_D < r$, an energy barrier results (for the full modelling, see [14]; the case in which the opposite situation is present, $\lambda_D > r$, would be modelled by the case of fully depleted grains with no

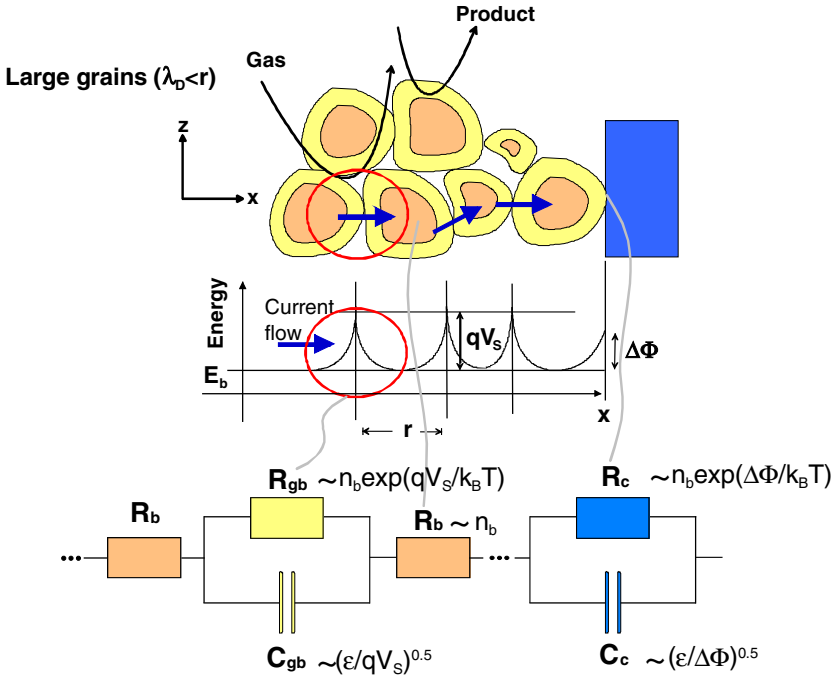

Figure 12. Equivalent circuit for the different contributions; intergranular contact, bulk and electrode contact. Intergranular contact: the ionosorption of oxygen at the grain surface results in the creation of a potential barrier and the corresponding depletion layers at the intergranular contacts. An intergranular contact can be represented electronically by a resistor R_{gb} (due to the high resistive depletion layers) and a capacitor C_{gb} (due to the sandwiching of high resistive depletion layers between two high conductive 'plates' of bulk material) in parallel. The electrode contact can also be represented by a (RC) element. The values of the resistor R_c and the capacitor C_c are independent of the ambient gas atmosphere. The bulk contribution can be represented by a resistor R_b, whose resistance value is hardly influenced by changes in the ambient atmosphere.

band bending described by simple resistors, see also [27]). The depletion layer thickness and the corresponding barrier height depend on the ambient gas atmosphere. A similar situation holds for the semiconductor–metal contact at the electrodes. However, in contrast to the grain–grain contacts, their Schottky barrier height is determined by the difference in the work functions of the metal and semiconductor and not by the surface processes (see [14]). Changes in the electron concentration near the metal–semiconductor contact due to the gas interaction at the SnO_2 grains are immediately compensated by electron transfer from the electrode and, as a result, the resistance of the metal–semiconductor contact does not depend on the ambient atmosphere.

The experimental results are presented in figures 13–16.

The results, which have been obtained by ac characterization, can be summarized as follows:

- The sensor impedance can be represented by an equivalent circuit consisting of a resistor, a (RCPE) element and, for dry air, an additional (RC) element, all in series (figures 13 and 14).
- For dry background air, the CO dependence of all resistive and capacitive elements of the equivalent circuit resemble those of an intergranular Schottky contact, i.e. the

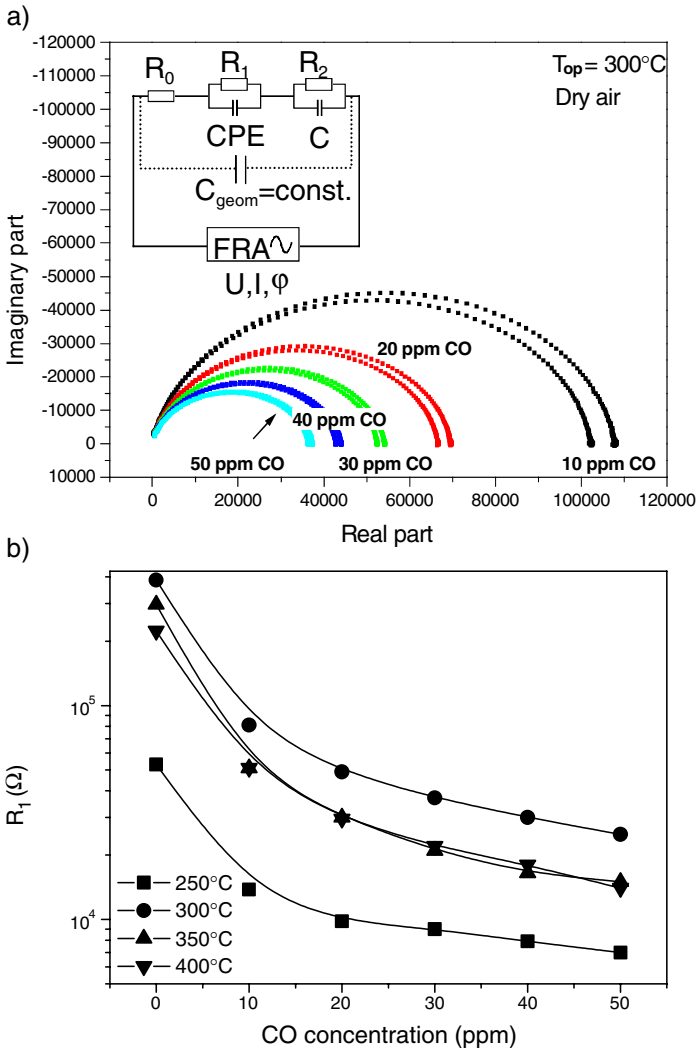

Figure 13. Equivalent circuit for the sensitive layer with dry synthetic air as background gas. (a) Impedance data in the Bode diagram for dry background gas. Two measurements have been performed for each CO concentration (0, 10–50 ppm). The data can be fitted nicely with an equivalent circuit consisting of a resistor (R_0), a R-CPE ($R_1 \parallel$ CPE) element and a (RC) element ($R_2 \parallel C$) parallel to the geometric capacitance C_{geom}. The resistances are in the $k\Omega$ range, while the capacitance and the CPE are in the pF range. The geometric capacity determined C_{geom} is constant for all ambient atmospheres and equal to the geometric capacitance of a bare substrate. (b) The resistance R_1 decreases for all operational temperatures with increasing CO concentration (0–50 ppm).

resistance decreases with increasing CO concentration, whereas the capacitance increases (see figures 13 and 15 and the formula in figure 12; the decrease of the band bending V_S decreases the resistance and increases the capacitance).

- For humid background air, the resistance behaviour resembles that for dry air, but the capacitive behaviour is different. For small CO concentrations the capacitance is decreased whereas for higher CO concentrations it is increasing as in the case of dry background

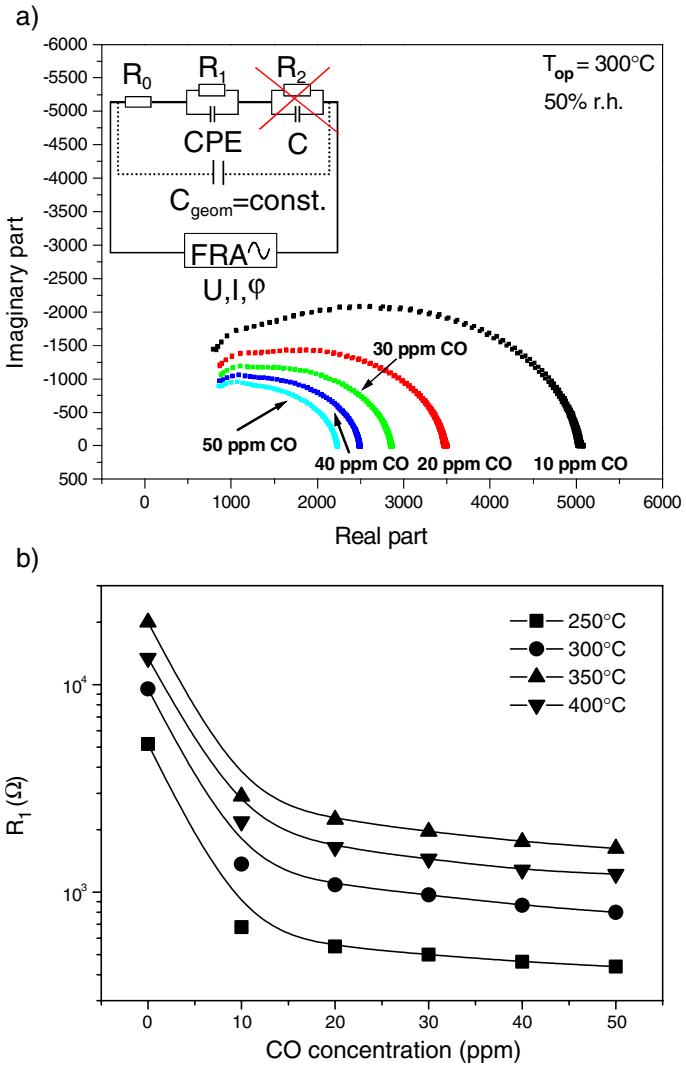

Figure 14. Equivalent circuit for the sensitive layer in the case of humid synthetic air as the background gas. (a) Impedance data in the Bode representation for humidified background gas. Two measurements have been performed for each CO concentration (0, 10–50 ppm). The data can be fitted nicely with an equivalent circuit consisting of a resistor (R_0) and a (R-CPE) element ($R_1 \parallel$ CPE) in parallel to the geometric capacitance C_{geom}. The resistances are in the $k\Omega$ range and the CPE are in the pF range. The determined geometric capacitance C_{geom} is constant for all ambient atmospheres and equal to the geometric capacitance of a bare substrate. (b) The resistance R_1 decreases for all operational temperatures with increasing CO concentration (0–50 ppm).

air (see figures 14 and 15). The 'strange' capacitive behaviour can be explained if one considers that, in the value of the capacitance of intergranular contacts, one also has the dielectric constant (see figure 12). For low CO concentrations, the water–CO reaction dominates, i.e. surface dipoles (OH groups) are removed from the surface and electrons are released into the grains. This is in line with the observed decrease in resistance. The reason for the observed capacitance decrease is the decrease of ε associated to the decrease

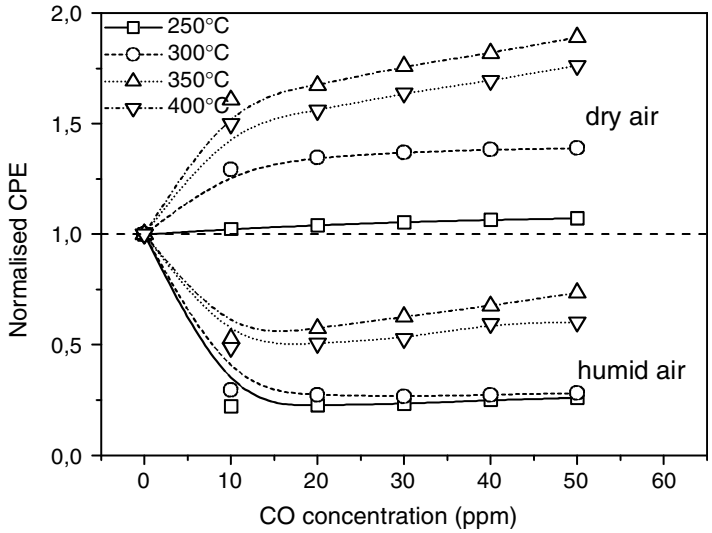

Figure 15. Normalized values of the CPE in a background of dry and humid air (50% relative humidity) for exposure to CO (0–50 ppm). In the case of dry air as the background gas, the CPE value increases monotonically with increasing CO concentration. In the case of humid air (50% relative humidity) as the background gas it decreases at first when exposed to 10 ppm CO and then increases with increasing CO concentration. For CO concentrations above 20 ppm, the curves in dry and humid air are approximately parallel.

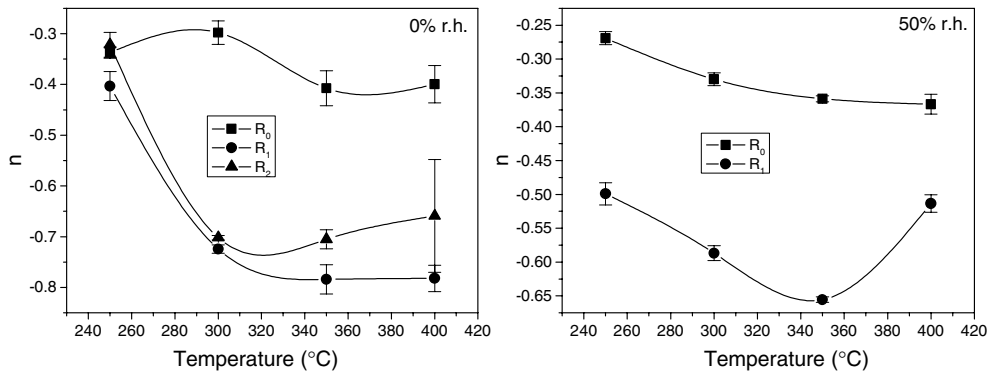

Figure 16. Influence of the operational temperature on the different resistors in the equivalent circuit for dry air (left) and humid air (right) as the background gas. The resistance behaviour of the various resistors in the presence of CO has been characterized by the power law exponent n. The power law exponents have been obtained by fitting the resistance curves of a resistor as a function of the CO concentration with a power law ($R = R_0 p_{CO}^{-n}$). The error bars in the plots represent the standard deviation of the fitting values. The power law exponent of R_0 decreases slightly with increasing temperature, whereby the behaviour is similar for dry and humid air. The power law exponent dependence of the other resistors on the operation temperature is significantly different. However, the behaviour of the exponents in dry air again resembles the exponent behaviour in humid air.

of surface dipole concentration, which is dominant at low CO concentrations. One assumes that in the capacitance change the driving factor is the change in the dielectric constant ε (which decreases the capacitance) and not the change of band bending V_S (which, as already described, increases the capacitance). For higher CO concentrations, the CO–

oxygen reaction dominates, which means that the dominant factor is the decrease of the band bending V_S. Accordingly the resistance is decreased and the capacitance is increased exactly as in the dry case, so the curves in dry background gas and in humid background gas become parallel with increasing CO concentration.

- The different behaviours in dry and humid background air confirm the hypothesis resulting out of the work function measurements of a dominant OH–CO interaction for low CO concentrations (ε-effect) and a dominant CO–O interaction for high CO concentrations (V_S-effect).

The resistance dependence on the CO concentration can be described by a power law function ($R \sim p_{\mathrm{CO}}^{-n}$) in the examined concentration range (10–50 ppm CO) for all resistors R_0 to R_2 (one has to remember that R_0 appears without a capacitive term, which could indicate that it is not associated with a depletion region). If the exponents are plotted for both dry and humid background air as a function of the operational temperature (figure 16), the exponents for R_0 and R_1 in dry background air resemble those for humid background air. Moreover, the exponent behaviour of R_2 greatly resembles the exponent behaviour of R_1. The exponent values for R_1 and R_2 are strongly affected by changes in the operational temperature, whereas for R_0 the exponent changes only slightly with operational temperature. Based on these results, it is plausible to assume that, for both dry and humid background air, there are two contributions within the sensitive layer, which behave qualitatively differently. These two contributions might be related to two different regions within the layer or to two different types of contribution, which are distributed more or less homogeneously within the layer. R_2, which only appears in dry background air, shows a similar CO dependence to R_1. It is likely that, in the case of humidified background gas, the humidity masks the presence of R_2 in the fit, for example, resulting in a more narrow distribution of the grain boundary characteristics reflected by only one (RC) element.

Before, it was assumed that all resistors R_0 to R_2 are related to Schottky barriers at the grain boundaries. The qualitative difference in CO dependence should thus be related to two different types of grain–grain interconnections or to grain boundaries with two different surroundings. However, theoretical calculations [42, 43] show that a distribution of the energy barriers around a mean value can be approximated by an effective barrier height $q \cdot V_S^{eff}$. Therefore, the CO interaction and thus the power law exponent should not be affected.

The observed difference in the power law exponent of the resistors R_0 and R_1 (R_2) could then be related to a change in the reactivity. If this is the case, a difference in the surroundings must cause this change in reactivity. One explanation would be that the surface of SnO_2 grains, which are rather close to the Pt electrodes, might be populated—due to the catalytic activity of the electrodes—with a different concentration of reactive species than those which are rather distant from the electrodes.

Another possible interpretation for the presence of different reactivities would be a mixture of partly and completely depleted grains. In this case the different surroundings of the grain–grain interconnections are the depleted ($r < \lambda_D$) or partly depleted grains ($r > \lambda_D$) with which they are connecting. As presented in [14], depleted grains and partly depleted grains would also give rise to different power law exponents. Also, completely depleted grains should appear only as a resistor in the equivalent circuit due to the lack of a Schottky capacitance. The CO dependence of the resistor can be described by a power law whose exponent is smaller than that of partly depleted grains. This is in accordance with what has been observed for R_0 in relation to R_1 and R_2.

There are a few elements that indicate that the first explanation might be the right one. First of all, the above-mentioned effect of Pt electrodes on the CO catalytic conversion. In

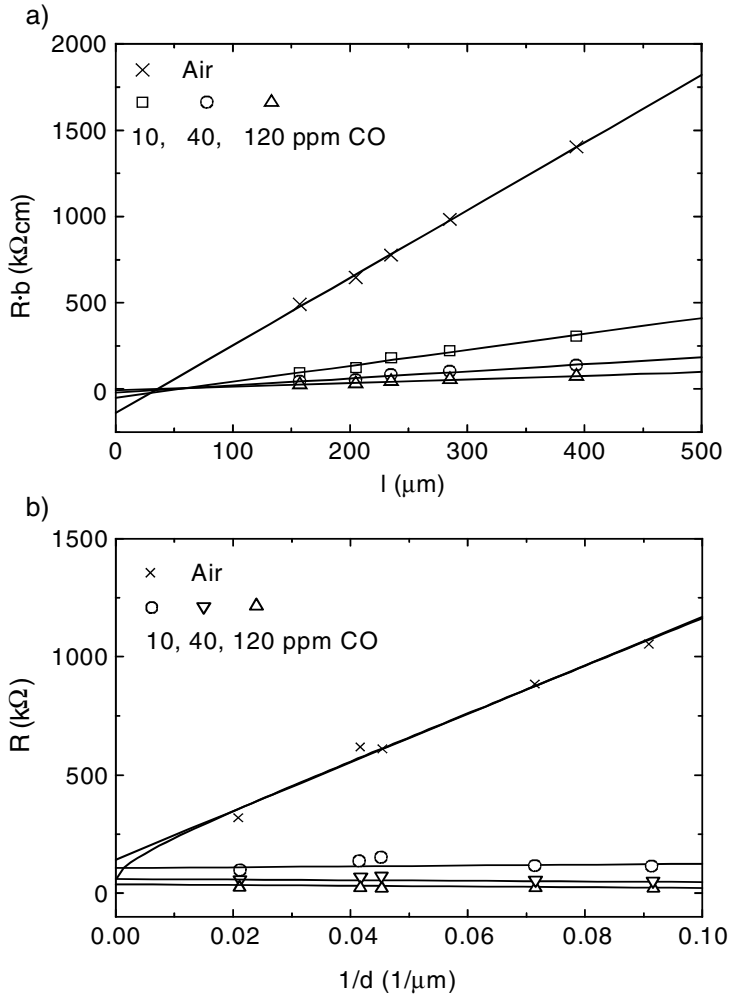

Figure 17. Dependence of the sensor resistance in air and in 10, 40 and 120 ppm CO on the sensor geometry as determined by Bauer *et al* [23]. The measurements have been performed in 50% relative humidity. (a) Dependence on the layer length l. (b) Dependence on the layer thickness d.

addition, results obtained by Bauer *et al* [23] on similar thick film sensors, where the sensitive layer of these sensors is based on doped SnO_2 and has been deposited by screen printing on an identical alumina substrate, may provide additional information on the results discussed previously. Figure 17 presents the influence of the geometry on the sensor resistance in air or CO (10–120 ppm). The sensitive layer deposited can be approximated as a parallelepiped. Transmission line measurements have been performed on the layer, i.e. the resistance of the layer has been determined for various electrode distances and thus various sample lengths l. With increasing sample length l, the resistance in air and in CO increases in a linear fashion as one would expect from

$$R = \frac{\rho l}{bd} \tag{15}$$

with l = layer length, b = layer width and d = layer thickness.

If, on the other hand, the layer thickness d is reduced from 100 to 5 μm, only the resistance in air changes as expected. In contrast to this, the resistance in CO remains unchanged. As a consequence, the resistivity ρ cannot be homogenous throughout the layer. It is reasonable to assume that a partial layer with resistance and a thickness of $d < 5$ μm determines the resistance in the case of CO exposure. A further increase in the total layer thickness does not change the layer resistance. Therefore the resistivity of the added part has to be significantly larger. The total layer can be divided into three partial layers: a layer at the top which is in direct contact with the gas atmosphere, a layer in the middle which is reached after gas diffusion and a layer at the bottom which is in direct contact with the substrate. With increasing thickness, the thickness of the intermediate layer is increased. Therefore it is plausible to assume that either the top or the bottom layer is the layer which has the characteristically low resistivity under CO exposure. In another experiment on the same sensors Bauer *et al* [23] investigated the dependence of the response time and the recovery time for CO exposure on the layer thickness. They found that the response time increases in a linear way with the layer thickness. This is a hint that the layer on the bottom plays the main role in the case of CO detection and that the gas has to reach the bottom layer before the equilibrium response can be achieved. These results emphasize once more the significant influence of the substrate on the gas sensing properties.

On the basis of the results obtained from the phenomenological sensor characterization, the sensing of CO in the presence of water vapour seems to be described as follows:

(1) CO sensing on tin oxide sensors is associated with consumption forming CO_2. The consumption is a linear phenomenon. The power law dependence of the resistance on the CO concentration is due to the transduction dominated by Schottky barriers.
(2) Water adsorption results in the formation of:
    - hydroxyl groups bound to Sn atoms forming strong surface dipoles and hence leading to changes in the electron affinity;
    - donors attributed to 'rooted' hydroxyl groups.
(3) Oxygen adsorption results in temperature-dependent ionosorbed species (O_2^-, O^{2-} and O^-), with O^- dominating in the range of interest (250–400 °C)
(4) CO sensing occurs via two pathways:
    - reaction with ionosorbed oxygen and
    - reaction with hydroxyl groups, which changes the electron affinity and releases H atoms. The latter combine with lattice oxygen and provide donors (rooted hydroxyl groups), i.e. free charge carriers.

    For lower concentrations and temperatures the reaction with OH groups dominate.
(5) The resistance dependence—of the equivalent circuit resistors corresponding to the different elements in the sensing layer—on the CO concentration for both dry and humid background air can be described by a power law ($R \sim p_{CO}^{-n}$) and resemble each other. The dependence of the exponent on the operational temperature can be related to two qualitatively different contributions to the layer resistance. These two contributions could be due to tin dioxide grains close to and further away from the catalytically active electrodes or due to the existence of depleted and undepleted grains.
(6) The overall consumption of sensors is not an independent combination of the contributions of the different sensor parts. The presence of the substrate influences the consumption of the sensitive layer. The effect of the sensor signal and the sensitive layer in contact with the Pt electrodes increases with increasing water vapour content of the gas.

For the validation of the modelling, additional spectroscopic measurements were performed.

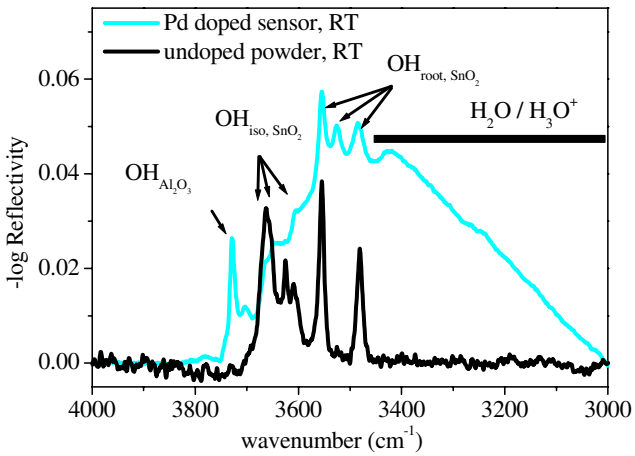

Figure 18. DRIFT spectra of a sol–gel SnO_2 powder and of the Pd doped sensor in the OH range at room temperature.

3.6. DRIFT measurements

The DRIFT spectra of sensors can be divided into three regions with their characteristic bands (for experimental details and complete results, see [19]):

- the region between 4000 and 3000 cm^{-1}: the stretching mode of hydroxyl groups and water-related species,
- the region between 2700 and 2000 cm^{-1}: hydrated proton species, CO and CO_2 in the gas phase, physisorbed CO and CO_2,
- the region between 2000 and 1000 cm^{-1}: unidentate, bidentate carbonates, carboxylates, oxygen ions, the deformation mode of water-related species and the absorption of free charges.

As an illustration, figure 18 shows RT DRIFT spectra of a powder prepared by a sol–gel method with a grain size of 100 nm and of a Pd doped sensor in the region between 4000 and 3000 cm^{-1} (the baseline was performed by using the spectra of KBr powder and of a KBr layer deposited over a sensor substrate). This comparison was necessary in order to:

- assess, by comparison with the well known and accepted use of the DRIFT technique on powders, the correctness of our results,
- to evaluate the differences originating from the sensor substrate.

One can see that several bands corresponding to the surface hydroxyl groups from the spectra of the sensor and the powder are overlapping. The bands at 3660, 3623 and 3608 cm^{-1} correspond to the isolated OH groups from tin dioxide (Sn–OH) while the bands at 3555, 3525 and 3484 cm^{-1} correspond to the tin dioxide rooted hydroxyl groups (O_O–H). This indicates that what we are measuring is coming from the SnO_2 sensitive layer.

However, in this region we also see differences. For example, a sharp band at 3728 cm^{-1}, not detected in the powder, can be assigned to hydroxyl groups observed on the alumina substrate [44, 45]. The occurrence of this additional band is due to the fact that the penetration depth of the IR radiation is in the range of millimetres and the thickness of the sensitive layer is 50 μm only; accordingly, we will also gain information related to the species adsorbed on the substrate. Also, the band at 3522 cm^{-1}, corresponding to the one for the rooted OH group,

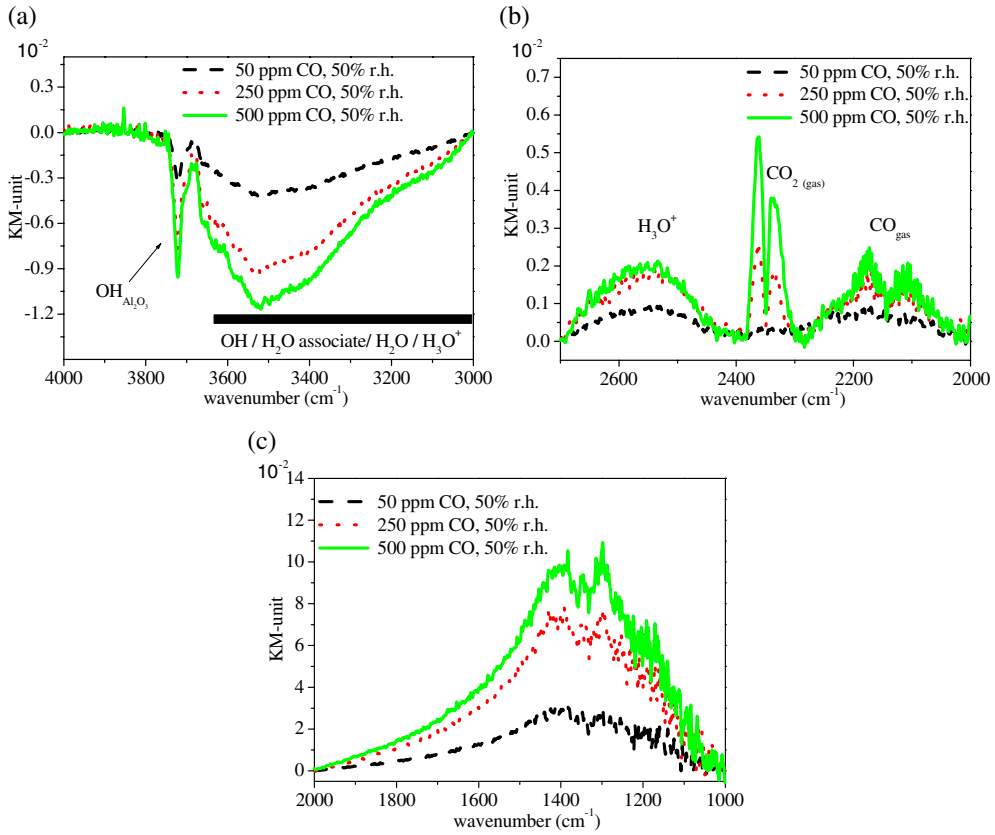

Figure 19. DRIFT spectra of Pd doped sensor at different CO concentrations in humid air; the different spectral ranges are shown separately.

and the broad band corresponding to the coordinated water/hydrated proton species belonging to the SnO_2 were not observed in the spectrum of the powder. The latter differences are most probably caused by the different pre-treatments of the powder and sensor and by the different surface properties of the compared SnO_2.

In the recorded DRIFT spectra of the sensor a general increase of absorption can be seen: it is caused by the absorption on free charges and almost completely masks all useful information between 2000 and 1000 cm^{-1}. As an example, figure 19 presents the effect of CO adsorption in the presence of humidity on the DRIFT spectra of the Pd doped sensors (for the baseline correction the spectra of the sensor before CO exposure was used as reference). In the presence of water the isolated hydroxyl groups on SnO_2 are becoming broader and show a shift towards lower wavenumbers. This fact indicates an association of the hydroxyl groups to water molecules most probably through hydrogen bonds. Hydroxyl groups on alumina do not show the same trend (no broadening and shifting of this band) (figure 19(a)). The broad band belonging to the OH/H_2O associations shows a very marked decrease with the increase of CO concentration (more than one order of magnitude when compared to the dry case: results not shown here; for details, see [19]). The OH groups on alumina also show a decrease in intensity. Parallel to the decrease of the band intensity in the OH/H_2O region, a clear increase of hydrated proton species, CO_2 and CO in the gas phase (between 2700 and 2000 cm^{-1}) and

an increase of free charge concentration were observed. At 50% relative humidity the decrease of the hydroxyl group band intensity, the sensor signal and the concentration of the hydrated proton species, as well as the concentration of the free charges, are much higher upon CO exposure than in the case of dry air. In order to derive the correlation between the changes in the intensity of the different bands during CO exposure, a quantitative band analysis for Pd doped and undoped sensors was performed. (Measurements on undoped sensors are still being carried out and their detailed results will be published elsewhere.)

To summarize, the results for CO experiments on Pd doped sensors are:

- the reduction of the bands in the OH/H_2O region is much higher in humid air than in dry air, as well as the increase of the concentration of the hydrated proton species (between 2700 and 2000 cm^{-1}) and free charges (2000 and 1000 cm^{-1}). The reaction between surface oxygen ions and CO is most probably responsible for the changes of the resistance in dry air. In the presence of water, the reaction between CO and hydroxyl groups determines the creation of hydrated protons, which additionally increases the sensor signal. The exact role of Pd in the reaction mechanism is still unclear but, due to the fact that for undoped sensors we record a different effect of humidity, Pd should play a determining role. It is also important to note that hydroxyl groups present at the sensor surface do not seem to react with CO in the absence of water vapour; this fact indicates that the association between OH groups and H_2O is the condition necessary for reaction with CO.
- The creation of CO_2 is not in line with the expected sensitization in the presence of humidity. As shown in [17], the cause is the additional oxidation of CO on the Pt electrodes and heater, which does not influence the sensor response and which is inhibited by the presence of humidity.

The results of DRIFT studies suggest that the role of the donor is played by the hydrated proton and not by the rooted hydroxyl group as was assumed by only taking into account the phenomenological studies. This again indicates that spectroscopic knowledge is crucial to the understanding of gas sensing. Using only electrical studies it is not possible to distinguish between the surface species which can play the same 'electrical' role.

On the basis of the knowledge gained up to now, one will have to advance in the following directions:

- Improvement of the performance of the DRIFT method with the aim of gaining useful information in the spectral range where the absorption bands of oxygen ions, carbonates and carboxylates are present;
- Using knowledge of the nature of the reaction paths for the microscopic modelling of the elementary steps with the aim of determining the associated energetic (electronic) levels of the surface, adsorption complex, precursor state and free molecule, and understanding the role of dopants;
- The transformation of the microscopic knowledge of changes in concentrations and mobilities of free charge carriers and the sensor resistance dependence of the ambient atmosphere to be validated by phenomenological measurements.

4. Conclusion and outlook

This work demonstrates that gas sensors based on metal oxides are complex devices and that it is not possible to understand them in the absence of a systematic approach. Accordingly, such an approach was proposed and applied with a reasonable degree of success. The results

obtained up to now are the first steps in understanding the mechanism of gas sensing with metal oxide sensors starting with the mechanistic level and continuing with the transducer function.

There are still a number of specific topics to be investigated and clarified; however, the already acquired knowledge allows for the next advances, especially towards an understanding of the role of dopants. The open questions are currently under investigation following the proposed line of thinking.

We think that by using the methodology developed in this work it is possible to expand this approach to other model systems including different metal oxides and target gases (mixtures). It is important to remember that the identification of the research targets, the preparation of the samples needed and the use of the appropriate research methods are crucial steps in any such attempt. Accordingly, it seems to us that sensor science has to be elaborated by combining the interests and knowledge of sensor developers, sensor users and scientists aiming at basic understanding; all these experts should talk to each other for their mutual benefit. The users can clearly identify the relevant objectives, the developers can optimize the samples/sensors and the scientists will be able to acquire the knowledge needed for further advances. The latter will have to be validated by the development of better performing real world sensors able to be applied for solving relevant practical problems.

References

[1] Bârsan N, Schweizer-Berberich M and Göpel W 1999 Fundamentals and practical applications to design nanoscaled SnO_2 gas sensors: a status report *Fresenius J. Anal. Chem.* **365** 287–304

[2] Schierbaum K D, Weimar U and Göpel W 1990 Multicomponent gas analysis: an analytical approach applied to modified SnO_2 sensors *Sensors Actuators* B **2** 71

[3] Mizsei J and Harsanyi J 1983 Resistivity and work function measurements on Pd-doped SnO_2 sensor surface *Sensors Actuators* **3** 397

[4] Mizsei J and Lantto V 1991 Simultaneous response of work function and resistivity of some SnO_2-based samples to H_2 and H_2S *Sensors Actuators* B **4** 163

[5] Geistlinger H, Eisele I, Flietner B and Winter R 1996 Dipole- and charge transfer contribution to the work function change of semiconducting thin films: experiment and theory *Sensors Actuators* B **34** 499

[6] Lenaerts S, Honore M, Huyberechts G, Roggen J and Maes G 1994 *In situ* infrared and electrical characterization of tin dioxide gas sensors in nitrogen/oxygen mixtures at temperatures up to 720 K *Sensors Actuators* B **18/19** 478

[7] Gutiérrez J, Arés M, Horrillo M.C, Sayago I, Agapito J and Lopez L 1991 Use of complex impedance spectroscopy in chemical sensor characterization *Sensors Actuators* B **4** 359

[8] Gutiérrez F J, Arés L, Robla J I, Horrillo M, Sayago I and de Agapito J A 1992 Properties of polycrystalline gas sensors based on dc and ac electrical measurements *Sensors Actuators* B **8** 231

[9] Xingqin L, Chunhua C, Wendong X, Yusheng S and Guangyao M 1993 Study on SnO_2–Fe_2O_3 gas-sensing system by ac impedance technique *Sensors Actuators* B **17** 1

[10] Ovenston, Sprinceana D, Walls J.R and Caldararu M 1994 Effect of frequency on the electrical characteristics of tin–antimony-oxide mixtures *J. Mater. Sci.* **29** 4946

[11] Weimar U and Göpel W 1995 AC measurements on tin oxide sensors to improve selectivities and sensitivities *Sensors Actuators* B **26/27** 13

[12] Martinelli G, Carotta M.C, Passari L and Tracchi L 1995 A study of the moisture effects on SnO_2 thick films by sensitivity and permittivity measurements *Sensors Actuators* B **26/27** 53

[13] Labeau M, Schmatz U, Delabouglise G, Roman J, Vallet-Regi M and Gaskov A 1995 Capacitance effects and gaseous adsorption on pure and doped polycrystalline tin oxide *Sensors Actuators* B **26/27**

[14] Bârsan N and Weimar U 2001 Conduction model of metal oxide gas sensors *J. Electroceramics* **7** 143–67

[15] Bârsan N, Heilig A, Kappler J, Weimar U and Göpel W CO—water interaction with Pd-doped SnO_2 gas sensors: simultaneous monitoring of resistances and work functions *Conf. Proc. EUROSENSORS XIII, The Hague (The Netherlands)* pp 183–4

[16] Kappler J, Bârsan N, Weimar U and Göpel W Influence of water vapour on nanocrystalline SnO_2 to monitor CO and CH_4 *Conf. Proc. EUROSENSORS XI, Warschau (P)* pp 1177–80

[17] Kappler J, Bârsan N, Tomescu A and Weimar U 2001 CO consumption of Pd doped SnO_2 based sensors *Thin Solid Films* **391** 186–91
[18] Harbeck S, Bârsan N, Weimar U and Hoffmann V 2001 *In situ* diffuse reflectance infrared spectroscopy study of CO adsorption on SnO_2 *Thin Solid Films* **391** 176–85
[19] Harbeck S, Szatvanyi A, Bârsan N, Weimar U and Hoffmann V 2003 DRIFT and electrical resistance studies of thick film SnO_2 sensors: temperature changes effect and CO detection mechanism in the presence of water vapour *Thin Solid Films* submitted
[20] Bârsan N, Siciliano P, Kappler J, Vantaggio M, and Weimar U 2003 CO sensing with SnO_2 sensors in the presence of humidity as revealed by impedance spectroscopy measurements *Sensors Actuators* B submitted
[21] Kappler J, Bârsan N, Weimar U, Diègez A, Alay J L, Romano-Rodriguez A, Morante J R and Göpel W 1998 Correlation between XPS, Raman and TEM measurements and the gas sensitivity of Pt and Pd doped SnO_2 based gas sensors *Fresenius J. Anal. Chem* **361** 110–14
[22] Bârsan N, Stetter J R, Findlay M and Göpel W 1999 High performance gas sensing of co: comparative tests for semiconducting (SnO_2-based) and for amperometric gas sensors *Anal. Chem.* **71** 2512–17
[23] Bauer M, Bârsan N, Ingrisch K, Zeppenfeld A, Denk I, Schuman B, Weimar U and Göpel W 1997 Geometry and electrodes on the characteristics of thick films SnO_2 gas sensors; influence of measuring voltage *Proc. 11th European Microelectronics Conference (Venice, May 1997)* pp 37–44
[24] Riviere J C 1969 *Work Function: Measurements and Results in Solid State Surface Science* ed M Green (New York: Dekker) pp 179–289
[25] Tracy J C and Blakely J M 1968 A study of faceting of tungsten single crystal surfaces *Surf. Sci.* **13** 313
[26] Ihokura K and Watson J 1994 *The Stannic Oxide Gas Sensor Principles and Applications* (Boca Raton, FL: Chemical Rubber Company Press)
[27] Göpel W and Schierbaum K D 1995 SnO_2 sensors: current status and future prospects *Sensors Actuators* B **26/27** 1
[28] Williams D 1999 Semiconducting oxides as gas-sensitive resistors *Sensors Actuators* B **57** 1–16
[29] Heiland G and Kohl D *Chemical Sensor Technology* vol 1, ed T Seiyama (Tokyo: Kodansha) ch 2 pp 15–38
[30] Morrison S R 1990 *The Chemical Physics of Surfaces* 2nd edn (New York: Plenum)
[31] Henrich V A and Cox P A 1994 *The Surface Science of Metal Oxides* (Cambridge: Cambridge University Press) p 312
[32] Egashira M, Nakashima M and Kawasumi S 1981 Change of thermal desorption behaviour of adsorbed oxygen with water coadsoption on Ag+-doped Tin (IV) oxide *J. Chem. Soc. Chem. Commun.* 1047
[33] Bârsan N and Ionescu R 1993 The mechanism of the interaction between CO and an SnO_2 surface: the role of water vapour *Sensors Actuators* B **12** 71
[34] Ionescu R and Vancu A 1994 Time-dependence of the conductance of SnO_2:Pt:Sb in atmospheres containing oxygen, carbon monoxide and water vapour 1. Non-oscillatory behaviour *Appl. Surf. Sci.* **74** 207–12
[35] Schierbaum K D, Weimar U and Goepel W 1991 Conductance, work function and catalytic activity of SnO_2-based gas sensors *Sensors Actuators* B 205–14
[36] Tanaka K, Morimoto S, Sonoda S, Matsuura S, Moriya K and Egashira M 1991 Combustion monitoring sensor using tin oxide semiconductor *Sensors Actuators* B **3** 247–53
[37] Huyberechts G, Szecwka P, Roggen J and Licznerski B W 1997 Simultaneous quantification of carbon monoxide and methane in humid air using a sensor array and an artificial neural network *Sensors Actuators* B **45** 123–30
[38] Vancu A, Moise C, Tomescu A and Ionescu R 1999 Role of water vapour in the interaction of SnO_2 with CO and CH_4 *Sensors Actuators* B **61** 39–42
[39] Hahn S, Bârsan N and Weimar U 2001 Investigation of CO/CH_4 mixture measured with differently doped SnO_2 sensors *Sensors Actuators* B **78** 64–8
[40] Göpel W 1985 Chemisorption and charge transfer at semiconductor surfaces: implications for designing gas sensors *Prog. Surf. Sci.* **20** 9
[41] Yamazoe N, Fuchigami J, Kishikawa M and Seiyama T 1979 Interactions of tin oxide surfaces with O_2, H_2O and H_2 *Surf. Sci.* **86** 335
[42] Romppainen R and Lantto V 1988 The effect of microstructure on the height of potential energy barriers in porous tin dioxide gas sensors *J. Appl. Phys.* **63** 5159
[43] Sinkkonen J 1980 DC conductivity of a random barrier network *Phys. Status Solidi* b **102** 151
[44] Liu X and Truit R E 1997 DRIFT studies of the surface of gamma-alumina *J. Am. Chem. Soc.* **119** 9856–60
[45] Tsyganenko A A and Mardilovich P P 1996 Structure of alumina surfaces *J. Chem. Soc. Faraday Trans.* **92** 4843–52